19th Brazilian Congress of Thermal Sciences and Engineering
November 6th–10th, 2022, Bento Gonçalves - RS - Brazil

ENC-2022-0246
A TWO-DIMENSIONAL PARABOLIC MODEL FOR COMBUSTION CHAMBER SIMULATION

Erykson M. S. Costa
Marcio T. Mendonca
Fernando S. Costa
Instituto Nacional de Pesquisas Espaciais
EryckSonMarconny@gmail.com, marcio_tm@yahoo.com, fernando.costa@inpe.br
Cesar A. V. Salvador
Universidade Federal de Santa Maria
valverde@ufsm.br

Abstract.
Among the different propulsion systems used for attitude control, orbit correction and maneuvering of satellites, liquid bi-propellant thrusters present high specific impulses and can have thrust control. The development of these devices requires simulation models both for design and test bench planning and although nowadays there are comprehensive combustion models based on computational fluid dynamics, simple and fast models are required for preliminary studies. This paper presents a numerical model for the simulation of two-phase flows in combustion chambers based on the two-dimensional boundary layer equations in cylindrical coordinates. The liquid propellants are injected with known droplet size distributions into a recirculating flow of combustion products. The boundary layer equations are discretized using finite differences and marched downstream, considering droplet evaporation, mixing and combustion of propellant vapors with pre-existing gases. The evaporation model is based on a classic transfer number steady state formulation, where the droplet surface temperature is assumed close to the propellant boiling temperature. Burning of UDMH and NTO was simulated considering the formation of eleven product species (CO2, H2O, CO, H2, N2, O2, H, OH, O, NO, N). Results considering vaporization distance, temperature and velocity distributions, combustion gas composition and liquid propellant mass fraction along the chamber are presented considering a radial variation of fuel and oxidizer mass flow rates. The variation of vaporization length with equivalence ratio shows that, for the cases considered, the fuel vaporizes earlier than the oxidizer, and the radial distribution of the equivalence ratio determines if the core region or the wall region totally vaporises fuel first. The results considering different equivalence ratios correlate well with the resulting distribution of product species along the chamber. The choices of inlet equivalence ratio also have significant effect on the wall temperature. Velocity and temperature profiles show that the combustion close to the wall increase the mass flow and temperature such that the boundary layers thicknesses are very thin.

Keywords: *propulsion, combustion chamber reactive flow, boundary layer*

1. INTRODUCTION

Liquid propellant rocket engines (LPRE) can attain large trust levels and relatively high specific impulses when compared to solid propellant rocket engines. Storable propellants, such as hydrazine and hydrazine derivatives and mixtures, using nitrogen tetroxide (NTO) as oxidizer, are hypergolic and, consequently, do not require an ignition system.

Mathematical models for spray combustion are important for the development of combustion chambers. Those models allow comparative analysis of operation conditions and chamber configuration, reducing the number of experimental runs on test bench, cost and development time. There are a number of models for spray combustion available on the literature, with different levels of accuracy and complexity. Models based on the flow balance equations can be classified as one, two and three-dimensional models.

There are many initiatives in the development of numerical models to simulate two phase reactive flows in rocket combustion chambers. In 2001, sponsored by the European Office of Aerospace Research and Development, the German Center for Aerospace (DLR German Center for Air and Space-flight) organized a workshop aiming at the evaluation of CFD tools for simulation of spray combustion of cryogenic propellants (Oskar J. Haidn, 2001). The results presented

at the workshop and the provided test configurations were used latter by other investigators to access their models. For example Cheng and Farmer (2006) used those results to evaluate a multi-phase, real-fluid combustion model that was incorporated into a computational fluid dynamic model.

Earlier, in 1998, the complexities associated with modeling high-pressure mixing and combustion in rocket engines have been highlighted by Oefelein and Yang (1998). The problems raised by non-linear source terms in the balance equations, turbulence modeling, scalar mixing and real gas effects at high pressure were discussed and available modeling options at the time were presented, as well as simulation performance and accuracy aspects were treated.

Numerical simulations of propulsion include also hybrid rocket engines. Among other works available in the literature the work of Mazzeti and Barbante (2016) may be given as an example of the initiatives in this direction. They proposed to develop an accurate combustion model to obtain temperature distribution, axial velocity, mass fraction distribution, as well as regression rates. Their model consists on CFD turbulent simulation of the balance equations using a partially stirred reactor model. A similar model based on open source software was developed by Maya and Valdes (2018).

Other initiatives use commercial and in house CFD models coupled with multidisciplinary models in order to study thrust chamber cooling, including radiation, convection on both the combustor side and on regenerative cooling passages (Kang and Sun, 2011). These models may also include injector geometry details as well as droplet motion, heat transfer, evaporation and breakup using Lagrangian formulation (Kalmykov *et al.*, 2009; Xu *et al.*, 2020). Large eddy simulations for turbulent combustion and genetic algorithms couple with data base and reduced order models are also current practice (Raman and Hassanaly, 2019; Salvador and Costa, 2013; Riedmann *et al.*, 2019).

In spite of the remarkable advances in computational fluid dynamics of reacting flows, the use of simple and fast models are still relevant today for preliminary design of rocket engines combustion chambers. One-dimensional models are a first alternative to compute approximate averages of properties at each streamwise station of the combustion chamber in order to satisfy mass, momentum and energy balance. Salvador and Costa (2006) used an one-dimensional model in order to compare the performance of hydrazine and hydrazine mixtures burning with NTO in a multi-propellant combustion chamber. Two dimensional models are the next level of approximation and boundary layer equations are usually adopted to develop such models (Kuo, 1986). These models allow a more detailed description of the reactive flow on the combustion chamber.

The present investigation extends the work of Salvador and Costa (2006) by implementing boundary layer equations for the computation of the reactive flow through the combustion chamber. Mass, momentum and energy balance equations in two-dimensional control volumes at each section of the combustion chamber are solved. Two-dimensional volumes account for gradients in the radial direction, including mass, momentum and energy transport by diffusive processes. The two-dimensional model also allows the study of radial distribution of fuel and oxidizer mass flow rates and propellant spray parameters, important for wall cooling methodologies. The proposed two-dimensional model considers the combustion process in the chamber controlled by the liquid fuel and oxidizer evaporation rate. The important parameters to be determined are the vaporization length, the wall temperature for different equivalence ratios in the wall region, the combustion products composition and radial velocity and temperature profiles.

This paper is organized in four sections: Sec. 1. presents an introduction to the problem; Sec. 2. describes the methodology, which includes the computation of fuel and oxidizer droplet evaporation, chemical reaction of these reactants and determination of physical properties of the resulting combustion gases, and solution of the boundary layer evolution equations for mass, momentum and energy at each downstream station; Sec. 3. presents results in terms of wall temperatures, gas composition, velocity and temperature profiles, droplet evaporation length and evolution of the fuel to oxidizer ratio along the chamber; and Sec. 4. presents comments and conclusions.

2. METHODOLOGY

Figure 1 shows a combustion chamber scheme where fuel and oxidizer are injected forming two sprays with known droplet size distributions. The propellants vaporize, burn and mix with pre-existing combustion products, raising the gas temperature inside de chamber.

It is assumed that the combustion and gas mixture are much faster than the evaporation process. The resulting combustion gas composition is computed at each streamwise station for an equilibrium process at constant pressure and temperature.

Mass, momentum and energy balance equations are solved, given initial conditions at the combustion chamber entrance. The following hypothesis are considered:

1. two-dimensional axisymmetric, constant cross section combustion chamber,

2. process controlled by vaporization of droplets,

3. steady state condition and no volume forces,

4. viscous dissipation, Soret and Dufour effects negligible,

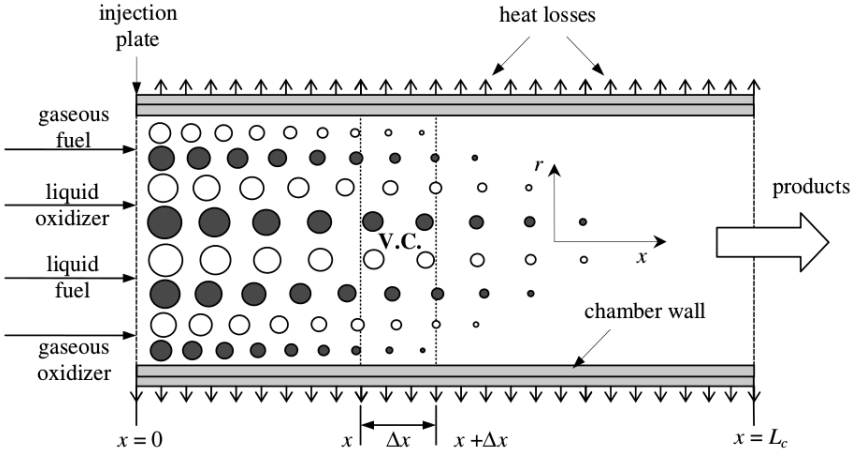

Figure 1. Combustion chamber model (Salvador and Costa, 2006).

5. diffusion between neighbour volumes in the radial direction,
6. negligible normal pressure gradient,
7. heat and momentum diffusion in the streamwise direction negligible, leading to boundary layer type equations

2.1 Balance equations

Considering that the balance equations may be simplified with boundary layer approximation, the following equations in cylindrical coordinates result,

Continuity equation

$$\frac{\partial \rho}{\partial t} + \frac{1}{r}\frac{\partial}{\partial r}\left(\rho r u_r\right) + \frac{\partial}{\partial z}\left(\rho u_z\right) = 0. \tag{1}$$

Where ρ is the density, t stands for time, r is the radial direction variable, z is longitudinal direction variable, u_r and u_z are the velocities in the radial and streamwise direction.

Streamwise and radial momentum equations

$$\rho\frac{\partial u_r}{\partial t} + \rho u_r\frac{\partial u_r}{\partial r} + \rho u_z\frac{\partial u_r}{\partial z} = -\frac{\partial p}{\partial r} + \frac{1}{r}\frac{\partial}{\partial r}\left(r\tau_{rr}\right) + \frac{\partial}{\partial z}\left(\tau_{rz}\right). \tag{2}$$

$$\rho\frac{\partial u_z}{\partial t} + \rho u_r\frac{\partial u_z}{\partial r} + \rho u_z\frac{\partial u_z}{\partial z} = -\frac{\partial p}{\partial z} + \frac{1}{r}\frac{\partial}{\partial r}\left(r\tau_{rz}\right) + \frac{\partial}{\partial z}\left(\tau_{zz}\right). \tag{3}$$

Newtonian stress tensor components equations

$$\tau_{rr} = \mu\left[2\frac{\partial u_r}{\partial r} - \frac{2}{3}\left(\frac{1}{r}\frac{\partial(r u_r)}{\partial r} + \frac{\partial u_z}{\partial z}\right)\right], \qquad \tau_{zz} = \mu\left[2\frac{\partial u_z}{\partial z} - \frac{2}{3}\left(\frac{1}{r}\frac{\partial(r u_r)}{\partial r} + \frac{\partial u_z}{\partial z}\right)\right], \tag{4}$$

$$\tau_{zr} = \tau_{rz} = \mu\left[\frac{\partial u_z}{\partial r} + \frac{\partial u_r}{\partial z}\right]. \tag{5}$$

Where μ is the dynamic viscosity coefficient

Energy balance equation,

$$\rho c_p\left(u_r\frac{\partial T}{\partial r} + u_z\frac{\partial T}{\partial z}\right) - \left(u_r\frac{\partial p}{\partial r} + u_z\frac{\partial p}{\partial z}\right) = \frac{1}{r}\frac{\partial}{\partial r}\left(kr\frac{\partial T}{\partial r}\right). \tag{6}$$

Where c_p is the specific heat at constant pressure, T is the temperature, k is the thermo conductivity coefficient.

Perfect gas equation of state

$$p = \rho R_u T\sum_{i=1}^{N}\frac{Y_i}{W_i}. \tag{7}$$

Where R_u is the universal gas constant, Y_i is the mass fraction and W_i is the molar mass and the mole fraction is

$$X_i = \frac{Y_i/W_i}{\sum_j\left(Y_j/W_j\right)}. \tag{8}$$

2.2 Initial and boundary conditions

At the injection plate liquid fuel and oxidizer are introduced with a known droplet size and mass flow rates. Known quantities of fuel and oxidizer mass flow rates are considered as already vaporized. No slip boundary conditions and adiabatic walls are considered at the chamber wall. Uniform initial conditions for velocity and temperature are the given for the boundary layer equations at the combustion chamber entrance.

2.3 Solution procedure

The parabolic balance equations presented above are solve numerically marching in the streamwise direction from given initial conditions. At each streamwise position the boundary layer equations are solved numerically for the velocity and temperature distributions with a second order finite differences backward scheme in the streamwise direction and a second order centered finite differences scheme in the radial direction. The gas composition and properties lag behind and are taken from the previous step.

Given the velocity and temperature fields at each computed streamwise position, the fuel and oxidizer evaporation are computed next and the same routine computes the composition of the resulting combustion. Liquid propellant evaporation are computed according to the methodology of Chin and Lefebvre (1983) and Lefebvre and McDonell (2017). Thermodynamic and physical properties are computed based on correlations found on NIST (https://www.nist.gov/), NASA CEA (https://cearun.grc.nasa.gov/), results from kinetic theory for gases (Law, 2006) and other sources (Svehla, 1995; Poling *et al.*, 1977; McBride *et al.*, 1993).

Then, the preexisting gases are mixed with the combustion products of the evaporated droplets in a thermodynamic equilibrium and mass conservation routine. Physical properties of the resulting gases are computed at that streamwise station and another step in the streamwise direction is taken. The process is repeated until either the fuel or oxidizer droplets are completely evaporated.

To start the computation the geometry of the combustion chamber, the fuel and oxidizer inlet areas and total mass flow rates are given, along with the liquid propellants temperature, combustion chamber pressure and amount of propellants already reacted at the chamber entrance, simulating a recirculation of gases in the combustion chamber.

Chemical equilibrium conditions are determined for the reaction of UDMH and NTO with formation of 11 chemical species: $CO_2, CO, H_2O, H_2, O_2, N_2, H, OH, O, NO$ and N.

3. RESULTS

The total fuel and oxidizer mass flow rates entering the combustion chamber $\dot{m}_f$, $\dot{m}_{ox}$, the resulting fuel/oxidizer mass flow ratio f and the equivalence ratio Φ are presented in Tab. 1, along with the combustion chamber geometry and pressure.

A percentage of the propellants is assumed to enter the combustion chamber and to evaporate and burn immediately. The temperature of these pre-existing gases at the chamber entrance is determined according to the equilibrium temperature of fuel/oxidizer combustion at the specified chamber pressure. It was assumed that 10% of the oxidizer evaporate immediately at the entrance with a fuel/oxidizer ratio $f = 0.85$ for the initial evaporation of fuel. For the initial conditions considered, the resulting temperature of the pre-existing gases is equal to 2125 K.

The total fuel to oxidizer mass flow rate condition $f = 0.4$, $\Phi = 1.2248$, at the inlet was taken as reference and the chamber was divided in two radial regions, a core region and a wall region. The core region takes 80% of the cross section area and the wall region the remaining 20%. Mass flow for the different cases consider mass flow rates 80%/20% split on the core and wall regions for the reference case. This reference case is compared with three different cases where, in the wall region the inlet mass flow rates were taken such that the inlet equivalence ratio Φ are equal to 0.7, 1.0 and 1.6. The equivalence ratio for each one of these values were given either by changing the fuel mass flow rate or the oxidizer mass flow rate, but the results between the two options did not vary significantly for the evaporation length, wall temperature or chemical composition of the burned gases.

The inlet mass flow rates and fuel to oxidizer ratio test cases are presented in Tables 1. Also shown in Tab. 1 are the vaporization length (the length for total evaporation of either the fuel or oxidizer), the temperature at the center of the core region ($r = 0$) and the temperature at the wall at the streamwise position where one of the propellants has already totally evaporated.

Figure 2 shows the vaporization length variation with equivalence ratio Φ, considering both the case when the inlet mass flow rate of the fuel was reduced and the oxidizer mass flow rate was kept fixed and the case when the inlet mass flow rate of the oxidizer was increased and the fuel mass flow rate was kept fixed. Changing the equivalence ratio by increasing the fuel mass flow rate for a fixed oxidizer mass flow, the vaporization length increases. For the lower values of Φ of 0.7 and 1.0 the fuel droplets evaporate first close to the wall and before the oxidizer droplets. For Higher equivalence ratios the fuel droplets evaporate before the oxidizer, first at the core region.

If the equivalence ratio is changed by fixing the fuel mass flow rate and changing the oxidizer mass flow rate, the

Table 1. Reactants mass flow rate, fuel/oxidizer equivalence ratio Φ, vaporization length x/L, core temperature and wall temperature at vaporization length x/L. Stoichiometric fuel/oxidizer ratio $f_s = 0.32658$. Fixed oxidizer mass flow rate for different fuel mass flow rates and fixed fuel mass flow rate for different oxidizer mass flow rates.

geometry and pressure $L = 80 \times 10^{-3}$ m, $D = 40 \times 10^{-3}$ m, $P = 20$ atm					
total mass flow, fuel/oxidizer ratio and equivalence ratio $\dot{m}_f = 22$ kg/s, $\dot{m}_{ox} = 55$ kg/s, $f = 0.4$, $\Phi = 1.2248$					
core region					
$\dot{m}_f$ kg/s	$\dot{m}_{ox}$ kg/s	Φ	x/L(vap)		
13.86×10^{-3}	39.60×10^{-3}	1.22	0.325		
wall region fixed oxidizer mass flow for different fuel mass flow					
$\dot{m}_f$	$\dot{m}_{ox}$	Φ	x/L(vap)	$T(core)$ K	$T(wall)$ K
2.51×10^{-3}	$11. \times 10^{-3}$	0.70	0.200	2990	3076
3.59×10^{-3}		1.00	0.275	3017	3034
4.40×10^{-3}		1.22	0.325	3018	3022
5.75×10^{-3}		1.60	0.325	3018	2833
wall region fixed fuel mass flow for different oxidizer mass flow					
4.40×10^{-3}	19.25×10^{-3}	0.70	0.250	3011	3062
	13.47×10^{-3}	1.00	0.300	3020	3020
	11.04×10^{-3}	1.22	0.325	3018	3022
	8.42×10^{-3}	1.60	0.300	3020	2835

fuel droplets evaporate before the oxidizer at the core region, except for $\Phi = 1.6$ when the oxidizer at the wall region evaporates first. This is because at $\Phi = 1.6$ the mass flow rate of the oxidizer is considerably lower and the vaporization length drops to $x/L = 0.30$.

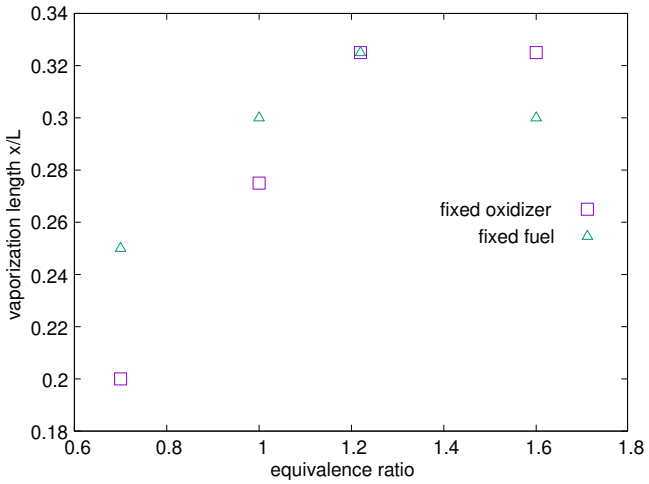

Figure 2. Vaporization length x/L versus initial equivalence ratio at the wall region. The equivalence ratio was changed either by changing the mass flow rate of the fuel and fixing the mass flow rate of the oxidizer, or vice-versa.

Figure 3 shows the temperature variation downstream close to the chamber wall for different values of the initial equivalence ratio. For $\Phi = 0.7$ the gas temperature increases with decreasing equivalence ratio along the chamber due to evaporation, since the pre-existing gases at 2125 K mixes with combustion gas. As the equivalence ratio decreases downstream due to different evaporation rates of fuel and oxidizer, the gas temperature continues to increase.

Increasing the equivalence ratio to $\Phi = 1.0$, increases the wall temperature significantly. Higher initial equivalence ratios ($\Phi = 1.22$ and $\Phi = 1.6$) result in lower temperature compared to $\Phi = 1.0$, but the equivalence ratio drops downstream to values as low as 0.4 and the resulting temperature downstream decreases. This effect will be shown bellow again in plots of radial temperature distribution as a function of equivalence ratio.

Given an initial liquid fuel to liquid oxidizer equivalence ratio at the chamber inlet, the evaporation of droplets along the chamber results in a streamwise variation of the propellant vapor equivalence ratio, as shown in Fig 4. This equivalence ratios correspond to the ratios between evaporated fuel and oxidizer.

The initial equivalence ratios considered are those of: a) a uniform distribution with $\Phi = 1.2248$ and b) non-uniform distributions with $\Phi = 1.2248$ at the core region and $\Phi = 0.7, 1.0$ and 1.6 at wall region.

Figure 4 shows that the resulting propellant vapor equivalence ratio varies significantly downstream when excess oxidizer is considered at the inlet ($\Phi = 0.7$). The equivalence ratio decreases downstream, resulting in an increase in gas temperature as the equivalence ratio is reduced towards values closer to the stoichiometric condition.

For the other initial equivalence ratios ($\Phi = 1.0$, 1.22 and 1.6) the streamwise variation of Φ are not so strong and the resulting gas temperature close to the wall increases as ϕ tends to the stoichiometric condition or decreases when it varies away from stoichiometry for $\Phi = 1.0$ as expected. Keep in mind that the temperature close to the inlet is influenced by the pre-existing gas temperature.

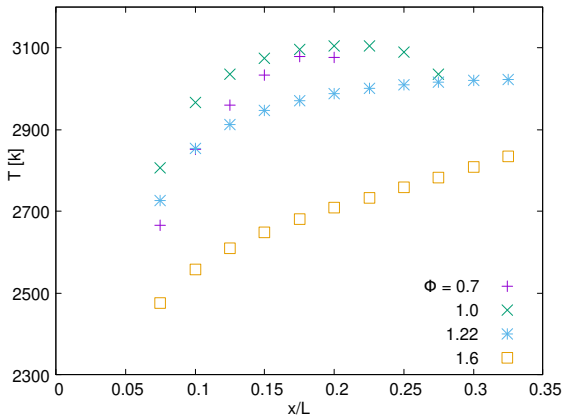

Figure 3. Temperature along the chamber in the region close to the wall.

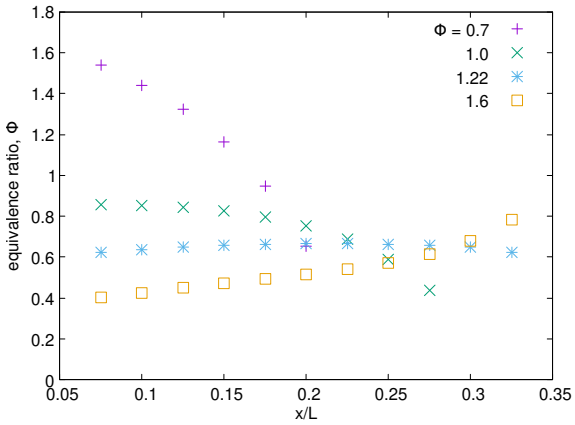

Figure 4. Equivalence ratio variation along the chamber in the region close to the wall.

To further understand the equivalence ratio variation downstream, figure 5 through 7 show the fuel and oxidizer liquid mass fraction ratio for the initial equivalence ratios $\Phi = 0.70, 1.0$ and 1.6, respectively. The different values of equivalence ratio for these test cases correspond to a given mass flow rate of oxidizer and increasing mass flow rates of fuel at the wall region, shown as the first group of conditions in Tab. 1.

The mass fraction ratio is defined as the ratio between the liquid mass at a streamwise station x and the total, fuel plus oxidizer, initial liquid mass at the chamber inlet at $x = 0$. Each plot also shows the reference case $\Phi = 1.2248$ where the equivalence ratio is uniform across the radial direction, both in the core and wall regions. All three plots show that, for any value of equivalence ratio Φ the oxidizer is consumed at a greater rate than the fuel, but since the amount of injected fuel is lower than that of the oxidizer, the fuel may be completely consumed before the oxidizer.

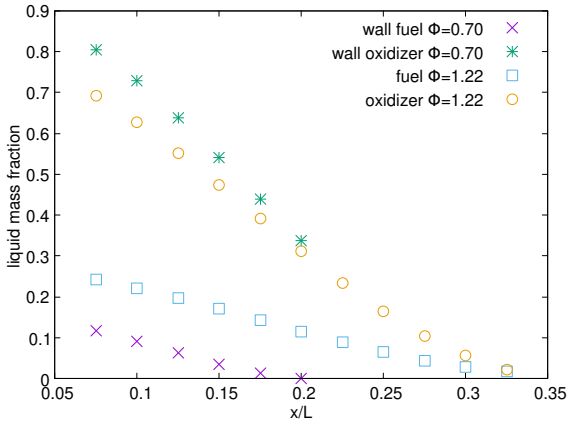

Figure 5. Liquid mass fraction variation along the combustion chamber both at the core and wall regions. $\Phi = 1.2248$ and 0.70.

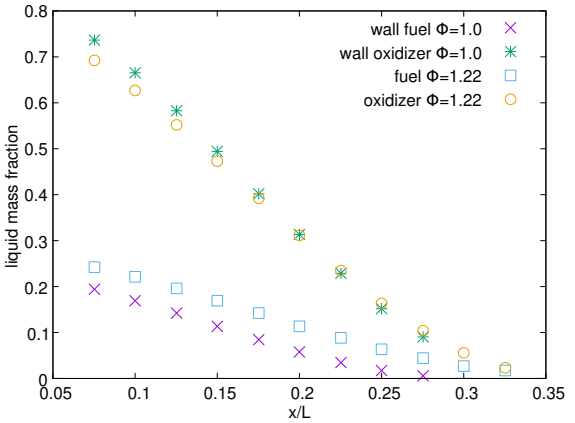

Figure 6. Liquid mass fraction variation along the combustion chamber both at the core and wall regions. $\Phi = 1.2248$ and 1.0.

For $\Phi = 0.7$, Fig. 5 shows that the fuel evaporates completely in the region close to the wall before the oxidizer. There is a considerable amount of remaining liquid oxidizer after the fuel has completely evaporated. The higher evaporation rate of oxidizer reduces the equivalence ratio downstream, as shown in Fig. 4, increasing the gas temperature, as shown in Fig. 3.

For the equivalence ratio of $\Phi = 1.0$ shown in Fig. 6, the trend is the same, but due to the higher initial amount of fuel, the fuel takes longer to fully evaporate and a greater quantity of oxidizer is consumed. On the other hand, for $\Phi = 1.6$ (Fig. 7) fuel and oxidizer are fully consumed at about the same streamwise position at the core region first, with remaining liquid propellants at the wall region. This is due to the greater amount of fuel at the wall region.

The increase in the equivalence ratio for initial $\Phi = 1.6$ is due to the greater fuel mass flow, which results in higher number of fuel droplets and, therefore, higher evaporated mass of fuel. This correlates well with the velocity plots shown bellow, where less quantity of burned gases result in lower velocities close to the wall, while for $\Phi = 0.70$ and 1.0, greater evaporation close to the wall result in higher velocities than that observed in the core region.

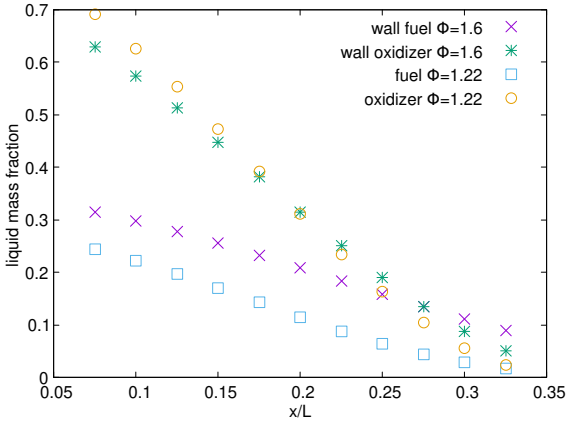

Figure 7. Liquid mass fraction variation along the combustion chamber both at the core and wall regions. $\Phi = 1.2248$ and 1.6.

Molar fraction variation along the length of the chamber in the wall region for CO_2, CO, H_2O and H_2 are shown in Figs. 8 to 11 below. Significant increase in CO_2 are observed for equivalence ratios higher than 0.7 due to a higher percentage of fuel in the evaporated mixture as shown in Fig. 4. The increase in the oxygen molar fraction close to the point where the fuel has already evaporated is expected due to the decrease of the local equivalence ratio for $\Phi = 1.22$ and 1.0 as also shown in Fig. 4. Molar fractions of CO, H_2O and H_2 decrease with increasing inlet equivalence ratio follow an opposite trend than that of CO_2. Down stream, the predominant gases are CO_2 and H_2O.

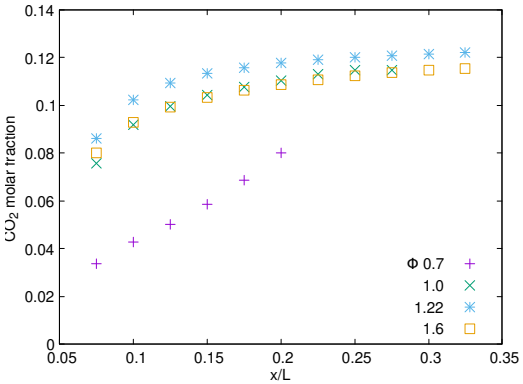

Figure 8. CO_2 molar fraction variation along the chamber in the region close to the wall.

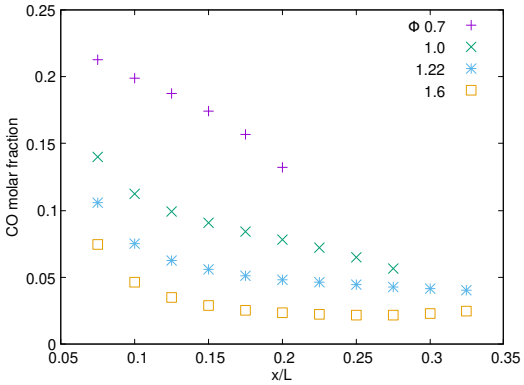

Figure 9. CO molar fraction variation along the chamber in the region close to the wall.

Next, temperature and velocity profiles in the radial direction at the streamwise position where the droplets have totally evaporated for each equivalence ratio are presented in Figs 12, 13 and 14. Each plot shows profiles for each equivalence ratio as well as profiles for the reference case where the equivalence ratio of $\Phi = 1.2248$ was imposed both at the core and wall regions.

As shown in Fig. 3, as the equivalence ratio increases the temperature close to the wall decreases. Given the adiabatic boundary condition at the wall and the combustion reaction in the region close to the wall, the resulting temperature distribution is mostly uniform and the wall temperature depends on the wall region reaction, without a significant thermal boundary layer region.

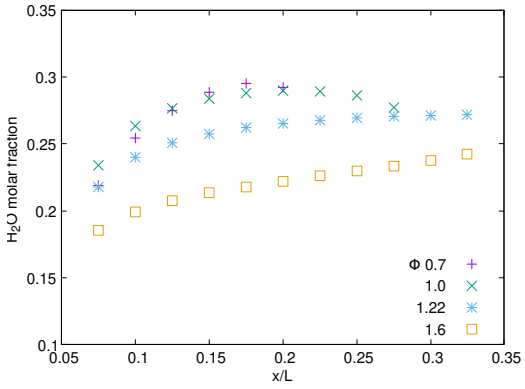

Figure 10. H_2O molar fraction variation along the chamber in the region close to the wall.

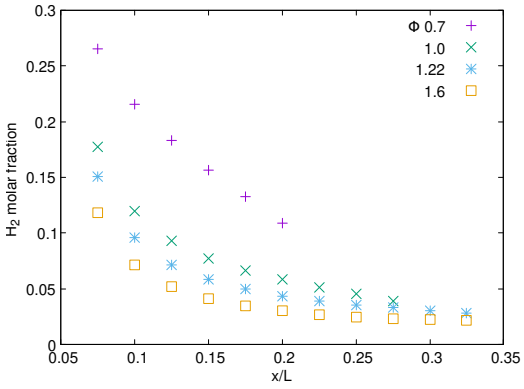

Figure 11. H_2 molar fraction variation along the chamber in the region close to the wall.

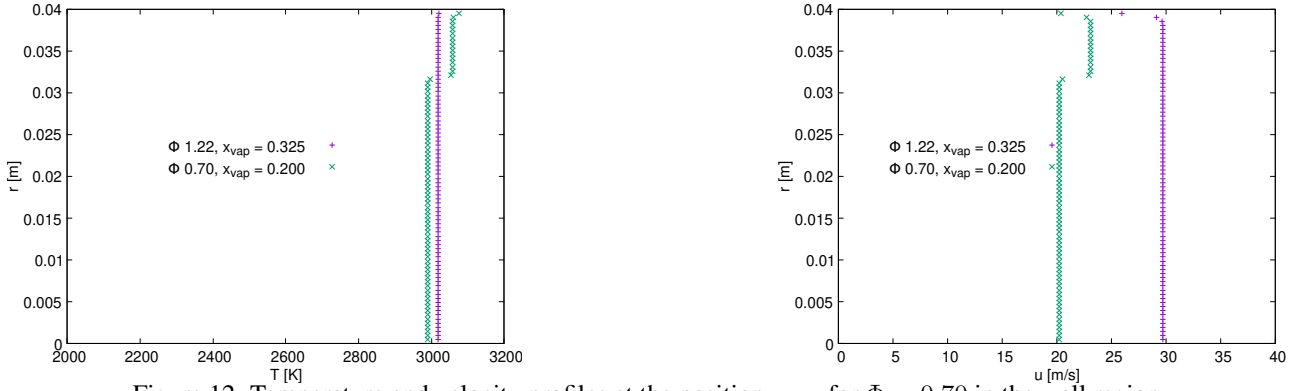

Figure 12. Temperature and velocity profiles at the position x_{vap} for $\Phi = 0.70$ in the wall region.

This same conclusion about the boundary layer thickness is also valid for the velocity profile, where the reaction of the evaporated propellants increase the mass flow rate of gases close to the wall and prevent the development of a thick boundary layer.

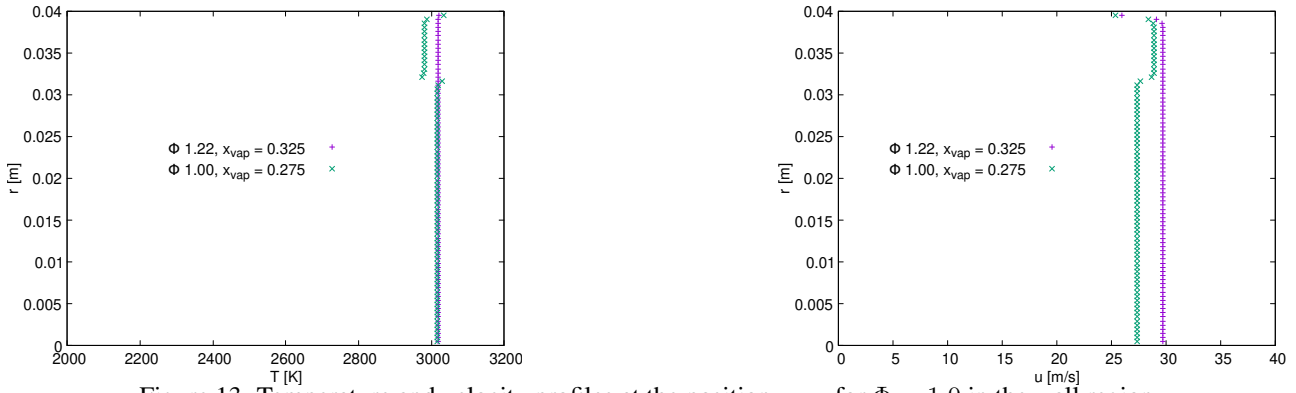

Figure 13. Temperature and velocity profiles at the position x_{vap} for $\Phi = 1.0$ in the wall region.

Comparison between different equivalence ratios results depends also on the vaporization length of each case, so that profiles are not compared at the same streamwise position. Nevertheless the effect of equivalence ratio variation from the core region to the wall region is clearly shown.

The temperature plots show that the wall region is not sufficiently resolved. This is because the grid spacing cannot be strongly refined or there will not be enough propellant droplets in the resulting small volume. At each grid control volume the number of droplets is proportional to the mass flow at that volume which cannot be made to small. Given that the boundary layer thickness is very thin due to the constant addition gas mass flow due to the burning of evaporated propellants, there is a balance between grid refinement to capture the boundary layer and grid spacing to allow a minimum number of droplets in the wall region.

The comparison of temperature levels at the core and wall regions is a function of the equivalence ratio through the combustion chamber in each region, which have different evaporation rates.

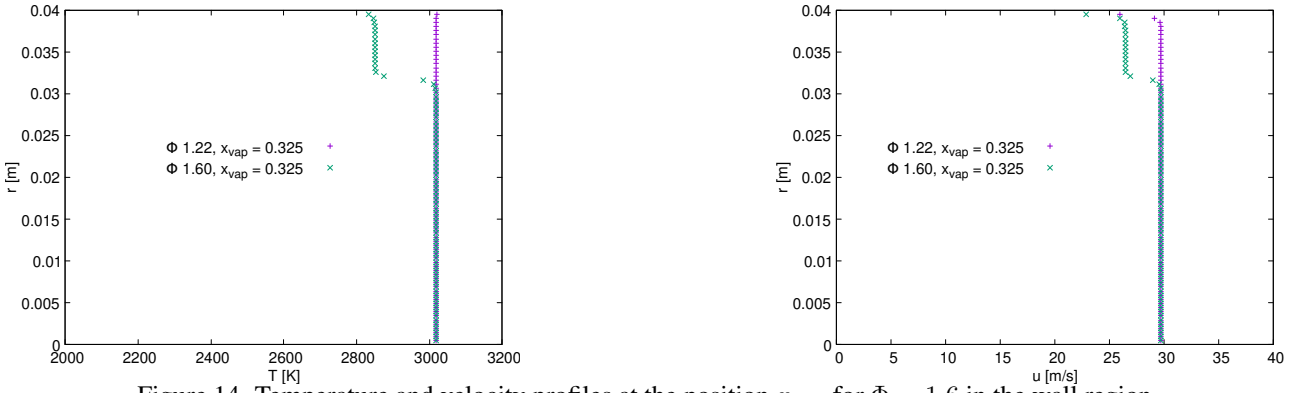

Figure 14. Temperature and velocity profiles at the position x_{vap} for $\Phi = 1.6$ in the wall region.

4. CONCLUSIONS

This paper describes a two-dimensional steady flow model for combustion chamber simulation, considering fuel and oxidizer droplets evaporation, with mixture and combustion of the resulting vapors. A radial distribution of equivalence ratio can be specified and increasing the equivalence ratio results in an increase in the vaporization length, which evaporates the fuel droplets before the oxidizer. The temperature close to the wall also increase with equivalence ratio, but as fuel is consumed the equivalence ratio downstream may decreases stabilizing the temperature. The effect of equivalence ratio on the distribution of molar fraction of the products results in higher amounts of CO_2, decreasing amounts for H_2O, CO and H_2 for equivalence ratios greater or equal to 1. The results also show that the boundary layer thickness is very thin due to constant addition of heat and mass flow close to the wall from combustion and that the wall temperature depends on the equivalence ratio.

5. ACKNOWLEDGEMENTS

The first author acknowledges the financial support from CAPES and the second author acknowledges the financial support from CNPq.

6. REFERENCES

Cheng, G.C. and Farmer, R., 2006. "Real fluid modeling of multiphase flows in liquid rocket engine combustors". *Journal of Propulsion and Power*, Vol. 22, No. 6, pp. 1373–1381.

Chin, J.S. and Lefebvre, A.H., 1983. "Steady-state evaporation characteristics of hydrocarbon fuel drops". *AIAA Journal*, Vol. 21, No. 10, pp. 1437–1443.

Kalmykov, G.P., Larionov, A.A., Sidlerov, D.A. and Yanchilin, L.A., 2009. "Numerical simulation of operation processes in the combustion chamber and gas generator of oxygen-methane liquid rocket engine". *Progress in Propulsion Physics*, Vol. 1, pp. 185–204.

Kang, Y.D. and Sun, B., 2011. "Numerical simulation of liquid rocket engine thrust chamber regenerative cooling". *Journal of Thermophysics and Heat Transfer*, Vol. 25, No. 1, pp. 155–164.

Kuo, K.K., 1986. *Principles of Combustion*. Wiley-Interscience, John Wiley & Sons, Inc., New York.

Law, C.K., 2006. *Combustion Physics*. Cambridge University Press.

Lefebvre, A.H. and McDonell, V.G., 2017. *Atomization and Sprays*. CRC Press, Taylor and Francis Group, 2nd edition.

Maya, E. and Valdes, J., 2018. "Numerical modeling of combustion process in hybrid rocket engines using open source software". American Institute of Aeronautics and Astronautics, AIAA, Ohio, USA, AIAA paper 2018-4438.

Mazzeti, A. and Barbante, P., 2016. "Numerical modeling of combustion processes in hybrid rocket engines". *International Journal of Energetic Materials and Chemical Propulsion*, Vol. 15, No. 3, pp. 249–2746. doi: 10.1615/IntJEnergeticMaterialsChemProp.2016013641.

McBride, B.J., Gordon, S. and Reno, M.A., 1993. "Coefficients for calculating thermodynamic and transport properties of individual species". Reference publication 4513, National Aeronautics and Space Administration, National Aeronautics and Space Administration. Lewis Research Center. Cleveland, Ohio 44135.

Oefelein, J.C. and Yang, V., 1998. "Modeling high-pressure mixing and combustion processes in liquid rocket engines". *Journal of Propulsion and Power*, Vol. 14, No. 5, pp. 843–857.

Oskar J. Haidn, e., 2001. "2nd international workshop on rocket combustion modeling". DLR and European Office of Aerospace Research and Development, DLR, Langer Grund Lampoldshausen, Germany.

Poling, B.E., Prausnitz, J.H. and O'Connell, J.P., 1977. *The Properties of Gases and Liquids*. The McGraw-Hill Compa-

nies, Inc. McGraw Hill Book Company, 5th edition.

Raman, V. and Hassanaly, M., 2019. "Emerging trends in numerical simulations of combustion systems". *Proceedings of the Combustion Institute*, Vol. 37, No. 2, pp. 2073–2089.

Riedmann, H., Banuti, D., Ivancic, B., Knab, O. and Hannemann, K., 2019. "Modeling of h2/o2 single-element rocket thrust chamber combustion at sub- and supercritical pressures with different computational fluid dynamics tools". *Progress in Propulsion Physics*, Vol. 11, pp. 247–272.

Salvador, C.A.V. and Costa, F.S., 2006. "Vaporization lengths of hydrazine fuels burning wih nto". *Journal of Propulsion and Power*, Vol. 22, No. 6, pp. 1362–1372.

Salvador, C.A.V. and Costa, F.S., 2013. "Large eddy simulation of bluff body stabilized turbulent premixed flame". *Journal of Aerospace Technology and Management*, Vol. 5, No. 2, pp. 181–196.

Svehla, R.A., 1995. "Transport coefficients for the nasa lewis chemical equlibrium program". Technical Memorandum 4647, NASA, National Aeronautics and Space Administration. Lewis Research Center. Cleveland, Ohio 44135.

Xu, J., Jin, P., Li, R., Wang, J. and Cai, G., 2020. "Effect of coaxial injector parameters on lox/methane engines: A numerical analysis". *Acta Astronautica*, Vol. 171, pp. 225–237.

7. RESPONSIBILITY NOTICE

The authors are solely responsible for the printed material included in this paper.